particles

MDPI

Article

Direct Photon Production in Heavy-Ion Collisions: Theory and Experiment

Dmitry Blau [1,2] and Dmitri Peresunko [1,2,*]

[1] National Research Centre "Kurchatov Institute", Moscow 123182, Russia
[2] National Research Nuclear University "MEPhI", Moscow 115409, Russia
* Correspondence: Dmitri.Peresunko@cern.ch

Abstract: Direct photons provide a possibility to test properties of hot matter created in proton–proton (pp), proton–nucleus (p–A) or nucleus–nucleus (A–A) collisions. As they are created in charged particles' scatterings and freely escape the hot region, they provide a tool to test all stages of the collision: the scattering of the partons of incoming nucleons, pre-equilibrium evolution and collective expansion of hot quark–gluon matter created in nucleus–nucleus collisions. Comparing direct photon production in pp, p–A and A–A collisions, one can check the scaling with the number of binary collisions expected at a high transverse momentum range and obtain insight into the hot and cold hadronic matter properties with soft photons. The collective elliptic flow of direct photons is a unique possibility to trace the collective flow formation and space–time evolution of the fireball. We review the experimental results on direct photon production in pp, p–A and A–A collisions at the Super Proton Synchroton (SPS), the Relativistic Heavy Ion Collider (RHIC) and the Large Hadron Collider (LHC) energies and discuss an agreement of theoretical predictions with measurements. Finally, we present predictions of direct photon spectra and collective flow for lower energy collisions expected at the Nuclotron-based Ion Collider fAcility (NICA) and the Facility for Antiproton and Ion Research (FAIR).

Keywords: heavy-ion collisions; direct photons; quark-gluon plasma; NICA; RHIC; LHC

Citation: Blau, D.; Peresunko, D. Direct Photon Production in Heavy-Ion Collisions: Theory and Experiment. *Particles* **2023**, *6*, 173–187. https://doi.org/10.3390/particles6010009

Academic Editors: Peter Senger, Arkadiy Taranenko and Ilya Selyuzhenkov

Received: 29 December 2022
Revised: 24 January 2023
Accepted: 25 January 2023
Published: 30 January 2023

1. Introduction

By measuring different properties of particles created in the ultra-relativistic nucleus–nucleus collisions, one can study hot quark–gluon matter, which is commonly referred to as quark–gluon plasma (QGP) [1]. Direct photons are the photons not originating from hadronic decays but produced in electromagnetic interactions in the course of the collision. Unlike hadrons, photons do not interact strongly with hot matter and thus provide information about all stages of the collision, as they are created at different times. At early times of the collision, prompt direct photons are produced in hard processes involving partons of incoming nucleons, such as Compton scattering, annihilation, bremsstrahlung or parton fragmentation. Once an (approximately thermalized) hot quark–gluon matter is created, thermal direct photons are radiated by it. These photons, having an approximately exponential spectrum, mainly occupy the low transverse momentum (low-p_{T}) part of the spectrum ($p_{\mathrm{T}} \lesssim$ 2–3 GeV/c), while prompt direct photons with a power-law spectrum dominate the high-p_{T} part. However, the main source of photons, contributing more than 90% of the total photon yield, is the decays of hadrons. This presents a challenge to measure direct photon spectra and correlations experimentally.

Below, we review available experimental results on direct photon production in high-energy proton–proton (pp) and proton–nucleus (p–A) collisions and discuss an agreement of these measurements with predictions of the perturbative quantum chromodynamics (pQCD) (Section 2). In Section 3, we discuss the direct photon production in nucleus–nucleus (A–A) collisions and the agreement of theoretical predictions with the experimental

measurements. Finally, in Section 4, we present predictions of the direct photon production at the energies of the future hadron accelerator facilities NICA and FAIR and discuss the peculiarities of the direct photon production at low colliding energies.

2. Direct Photons in High Energy pp and p–A Collisions

Direct photons created in high energy pp, p–A or A–A collisions can be split into two big classes: *prompt* direct photons produced in interactions of partons of incoming nucleons, and *thermal* direct photons representing the possible emission of hot matter created in the collision. Direct photons can be measured as the difference between an inclusive photon yield and a yield of decay photons calculated from the measured spectra of final hadrons, mainly π^0 and η mesons. Technically, this is a complicated experimental task, requiring a precise measurement of the neutral meson spectra. Instead, at high-p_{T} one can measure the spectrum of *isolated* photons, which are defined as photons without accompanying hadrons in a cone with a typical size of $\sqrt{\Delta\phi^2 + \Delta\eta^2} \sim 0.4$, where $\Delta\phi$ and $\Delta\eta$ denote the distance between a hadron and the photon in an azimuthal angle and pseudorapidity. This condition can be relatively easily implemented in an experiment, dramatically reduces a contribution of hadronic decays (and also of fragmentation and bremsstrahlung processes) and allows one to measure the isolated photon production on the event-by-event basis.

The PHENIX experiment was able to measure the spectra of direct and isolated photons simultaneously in pp collisions at the center-of-mass energy $\sqrt{s} = 200$ GeV [2] and confirmed the theoretical expectations that at low $p_{\mathrm{T}} \sim 5$ GeV/c there is a considerable, up to $\sim 50\%$, contribution of fragmentation and bremsstrahlung photons, but at high $p_{\mathrm{T}} \sim 15$, the GeV/c isolated photon spectrum almost coincides with the direct photon one and can be used as a good proxy for the direct photon spectrum.

A summary of direct and isolated photon spectra in pp and p–A collisions at different $\sqrt{s}$ is shown in Figure 1; see [3] for the references to the measured spectra. One can observe a universal scaling if spectra are plotted as a function of $x_{\mathrm{T}} = 2p_{\mathrm{T}}/\sqrt{s}$ and cross-sections are scaled by $(\sqrt{s}/\mathrm{GeV})^n$, with $n = 4.5$. First, note that the direct photon spectra measured with PHENIX, ALICE, E704, E706, NA24, WA70 experiments in this plot follow the same trend as isolated photon spectra (measurements of ATLAS, CMS, D0, CDF, UA1, UA2, UA6 experiments), confirming that isolated photons provide a good proxy for direct photons at high x_{T}. Some discontinuity at $x_{\mathrm{T}} \sim 3 \cdot 10^{-3}$ is related to the comparison of direct photon spectra containing additional bremsstrahlung and fragmentation contributions at lower x_{T} and isolated photon spectra at higher x_{T}. The second important observation concerns the power of n necessary for this scaling. The operator product expansion [4] allows one to classify processes according to a power of the hard scale. It suggests that for the $2 \to 2$ processes, the leading twist process should provide scaling $n \sim 4$, and contributions of the higher twist processes increase this power. The observed scaling with $n = 4.5$ for photons supports these speculations and appears to be smaller than the similar scaling of high-p_{T} hadron production [5], which led to the conclusion of the importance of higher-twist processes [6].

The yield of prompt direct photons can be calculated within perturbative QCD using structure functions of incoming nucleons, textbook cross-sections of parton scatterings and fragmentation functions of final partons. However, these calculations strongly underestimate the experimental results. A theoretical description of prompt photon production was dramatically improved thanks to the efforts of A.P. Contogouris et al. [7] and Gordon and Vogelsang [8], who proposed a technique to perform threshold and recoil resummations. These resummations were implemented in the Jetphox package [9], which demonstrated a good agreement with the data available at that time (see the review of measurements at SPS, Tevatron proton-antiproton collider (Tevatron) [10] and Hadron-Electron Ring Accelerator (HERA) [11]). A detailed comparison of the recent measurements of the isolated direct photons in pp collisions at the LHC energy is presented in Figure 2. The left plot represents measurements of the ATLAS collaboration in four rapidity regions up to very high $p_{\mathrm{T}} \sim 2000$ GeV/c. ATLAS data are compared to next-to-leading order (NLO)

calculations [10,12] with two recent parameterizations of structure functions and to next-to-next-to-leading order (NNLO) calculations [13]. The data agrees with the calculations with accuracies of about 10%. The right plot in Figure 2 shows the comparison of the low-p_T part of the isolated photon spectra measured by 3 LHC collaborations to theoretical predictions. Note that the definition of the isolated photons is slightly different from one experiment to another, and theoretical calculations are adjusted, respectively. Due to the dedicated design of the apparatus, ALICE was able to extend the previous measurements down to $p_T \sim 10\,\mathrm{GeV}/c$.

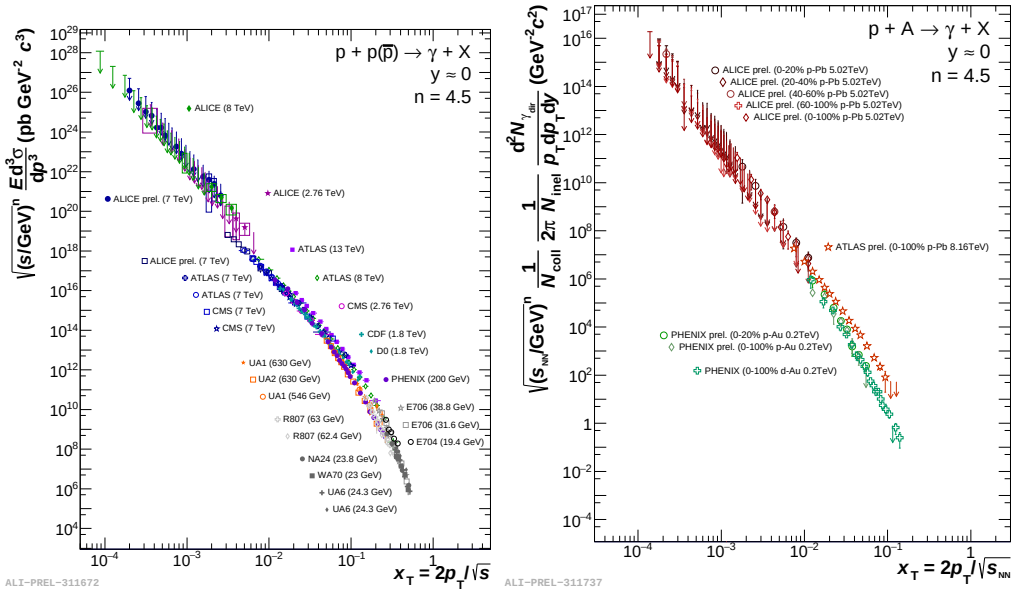

Figure 1. World data compilation of x_T-scaled direct and isolated photons spectra in pp($\bar{p}$) (**left**) and p–A (**right**) collisions. See [3] for the references to the measured spectra.

An extraction of prompt direct photons in p–A or A–A collisions proves that the very beginning of the p–A or A–A collision can be modelled as a combination of the N_{coll} nucleon–nucleon collisions, where the number of binary collisions N_{coll} can be estimated from the Glauber model [14]. Moreover, it allows one to constrain the possible modification of the nucleon structure functions in the nuclei. Note that if one uses pp data to estimate the prompt photon yield in A–A collisions at the same energy, one should take into account the isospin difference between protons and neutrons, which results in some decrease in the yield in A–A collisions at high x_T compared to the scaled pp spectrum [2]. Examples of direct photon spectra measured in Au–Au collisions at the center-of-mass energy per nucleon pair $\sqrt{s_{NN}}$ = 200 GeV (left) and Pb–Pb collisions at $\sqrt{s_{NN}}$ = 2.76 TeV (right) are presented in Figure 3. At the high-p_T part of the spectra, data are reproduced either by pQCD calculations or spectra measured in pp collisions at the same energy scaled with N_{coll}. Other measurements at LHC energies made by ATLAS [15] and CMS [16] collaborations also demonstrate a good agreement between measurements and N_{coll}-scaled pp predictions at a high-p_T region.

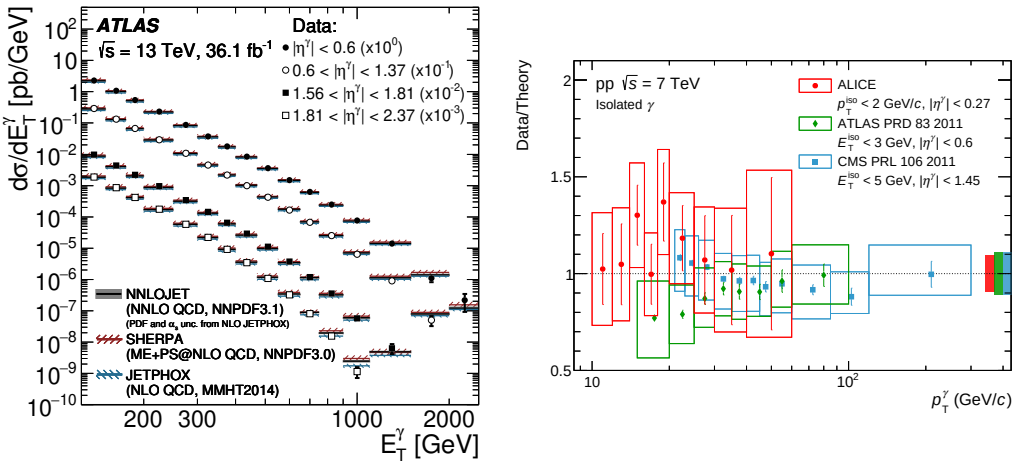

Figure 2. (**Left plot**): Isolated photon spectra measured by ATLAS collaboration in pp collisions at $\sqrt{s} = 13$ TeV in four rapidity regions compared to pQCD predictions [17]. (**Right plot**): Comparison of isolated photon spectra measured in pp collisions at $\sqrt{s} = 7$ TeV by three LHC experiments to theoretical predictions [18].

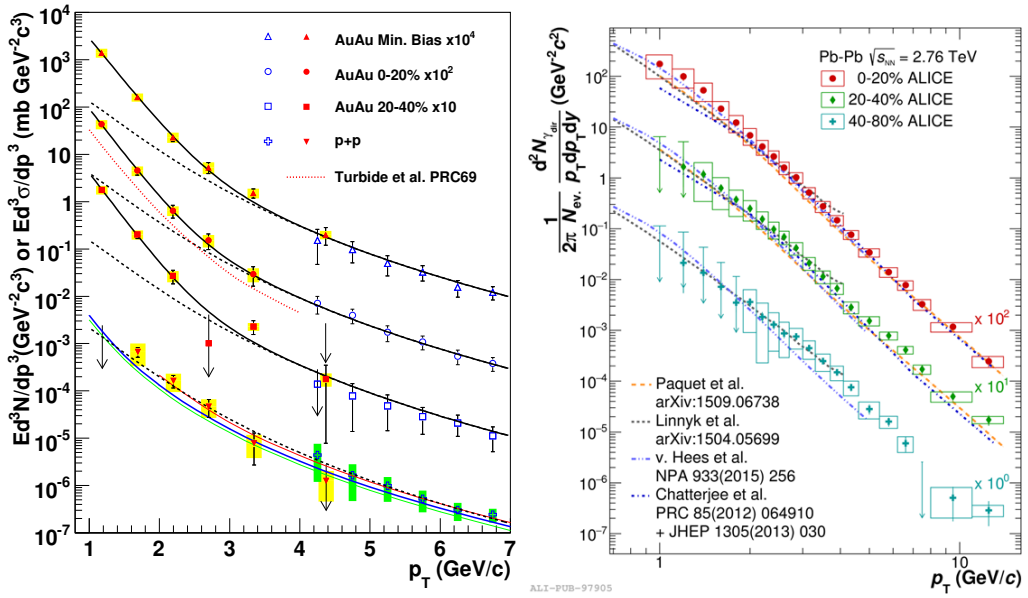

Figure 3. (**Left**): Direct photon spectra measured in Au–Au and pp collisions at $\sqrt{s_{\rm NN}} = 200$ GeV [19]. (**Right**): Direct photon spectrum in Pb–Pb collisions [20] at $\sqrt{s_{\rm NN}} = 2.76$ TeV.

3. Thermal Photon Production in High-Energy A–A Collisions

As it was discussed in the previous section, direct photon spectra measured in A–A collisions at RHIC and LHC energies, shown in Figure 3, demonstrate an agreement with prompt photon expectations at high-$p_{\rm T}$. At the same time, in the left plot one can clearly observe an excess of direct photons over the scaled pp yield at $p_{\rm T} < 3$ GeV/c. This excess is interpreted as a yield of thermal direct photons. In the right plot of Figure 3, a comparison of the direct photon spectra measured in Pb–Pb collisions at $\sqrt{s_{\rm NN}} = 2.76$ TeV with several models is presented. All models include the prompt photon contribution dominating at high $p_{\rm T}$ and thermal photon contribution. Theoretical calculations of thermal direct photons include either a hydrodynamic description of the evolution of hot matter (Paquet et al. [21], v. Hees et al. [22], Chatterjee et al. [23]) or the transport model PHSD (Parton-Hadron-String Dynamics) [24], with an accounting of the direct photon production. The measured

direct photon spectrum is somewhat higher than the model predictions, but is consistent, however, with the uncertainties.

The systematic comparison of the direct photon spectra measured in Au–Au collisions at $\sqrt{s_{\rm NN}} = 200$ GeV by PHENIX [25] and STAR [26] collaborations and preliminary ALICE results on Pb–Pb collisions at $\sqrt{s_{\rm NN}} = 5.02$ TeV with predictions of the same hydrodynamic model is presented in Figure 4. While STAR and preliminary ALICE results are consistent with the model predictions within uncertainties, the PHENIX measurements show a 2–4 times higher yield, both with respect to the STAR measurements at the same energy and hydrodynamic model predictions. The reason of this tension between two experiments is not clear so far. PHENIX implemented several experimental techniques to extract the direct photon spectrum: the internal conversion method [27] consists of the measurement of the di-electron invariant mass distribution at low $m_{\rm ee} < m_\eta$ and the extrapolation of the excess of virtual photons over the cocktail to the real photon spectrum using the Kroll-Wada relation [28]. The same method was used by the STAR collaboration in [26]. Moreover, the PHENIX utilized photon reconstruction in the electromagnetic calorimeter or via an e^+e^- pair produced as a result of a photon conversion on the detector material. Recently, PHENIX presented final direct-photon spectra in Au–Au collisions at $\sqrt{s_{\rm NN}} = 200$ GeV from the high-statistics 2014 data set [25]. A significant excess above the direct photon spectrum in pp collisions at $\sqrt{s} = 200$ GeV scaled by the $N_{\rm coll}$ is observed, and an agreement between different methods was confirmed.

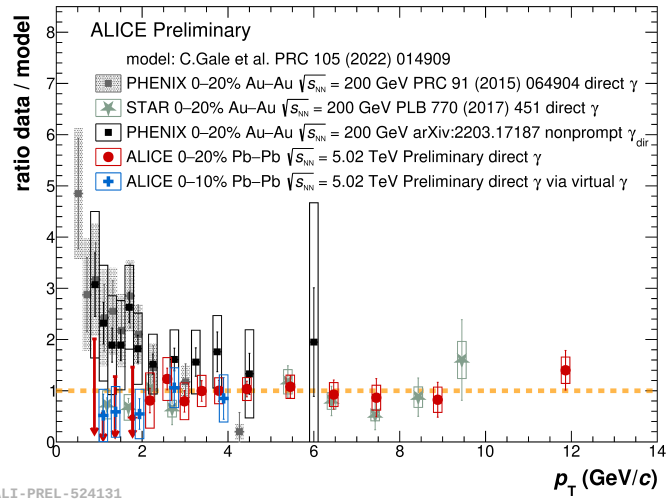

Figure 4. The ratio of direct photon spectra measured in Au–Au and Pb–Pb collisions for the hydrodynamic model predictions [29].

As the thermal photon yield was observed in A–A collisions at different energies, one can calculate the dependence of the integrated direct photon yield on the charged particles' multiplicity. The PHENIX collaboration performed a systematic study of direct photon production in Au–Au and Cu–Cu collisions at $\sqrt{s_{\rm NN}} = 39$, 64, 200 GeV. In all colliding systems, an excess of direct photons was observed. The summary of the integrated direct photon yield ($dN_{\gamma,\rm dir}/dy$) vs. charged particles' multiplicity ($\langle dN_{ch}/d\eta \rangle$) is shown in Figure 5. Data agrees with power-law scaling $dN_{\gamma,\rm dir}/dy \propto (dN_{ch}/d\eta)^\alpha$ with the power parameter $\alpha = 1.11 \pm 0.02$ (stat) $^{+0.09}_{-0.08}$(syst) [25]. The dashed line fits the previously published data, which provided $\alpha = 1.23 \pm 0.06$ (stat) ± 0.18(syst) [30], and the magenta band represents a fit to the $N_{\rm coll}$ scaled pp data.

As different stages of hot matter evolution can contribute to different $p_{\rm T}$ ranges, it is interesting to study the dependence of the integrated direct photon yield, starting from several minimal $p_{\rm T}^{\rm min}$, on the charged particles' multiplicity. Hydrodynamic calculations [31] predicted that the thermal emission from the hadron gas (HG) and from the QGP scale as $\alpha_{\rm HG} \approx 1.23$ and $\alpha_{\rm QGP} \approx 1.83$, respectively, while hard scattering contribution scales as $\alpha_{pQCD} \approx 1.25$. Thus, one could expect a strong $p_{\rm T}^{\rm min}$ dependence of the power parameter.

PHENIX, however, found that the $\alpha(p_T)$ is independent on p_T and equal to $\alpha \approx 1.1$; see Figure 6, left plot. This value is smaller than the power parameter $\alpha \approx 1.6$ expected for thermal photons; see Figure 6 in [31]. Thus, the low value of α may be related to an additional source of direct photons in these measurements, but uncertainties are still too large to make a firm conclusion here.

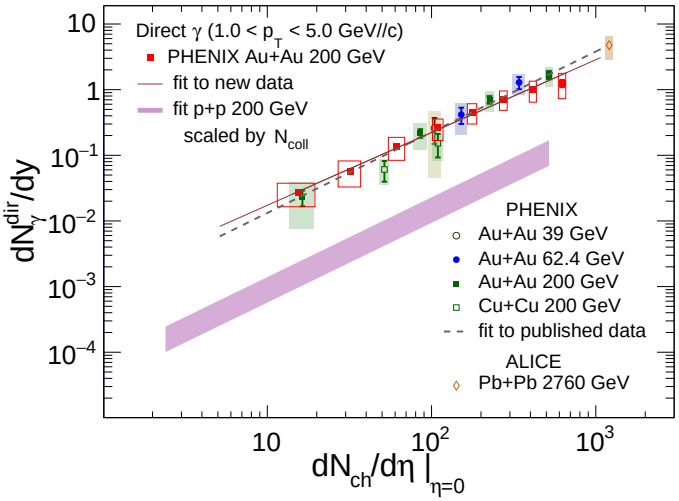

Figure 5. Integrated direct photon production in A–A collisions at different energies as a function of charged particles multiplicity [25].

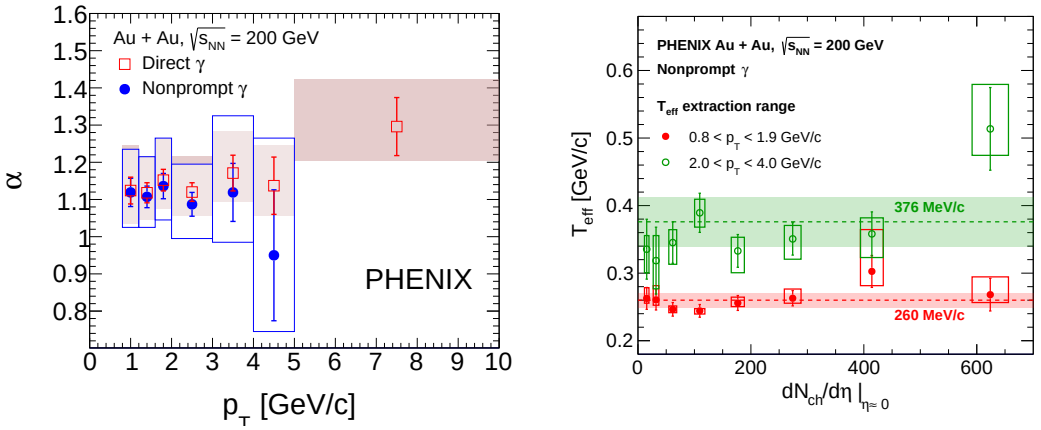

Figure 6. (**Left**): scaling parameter α as a function of minimal p_T used in the direct or thermal photon integrated yield calculation in Au–Au collisions at $\sqrt{s_{NN}} = 200$ GeV [25]. (**Right**): direct photon spectrum slope parameter, extracted in two p_T ranges, in Au–Au collisions at $\sqrt{s_{NN}} = 200$ GeV as a function of charged particles' multiplicity [25].

The effective temperature of thermal photons can be obtained as the inverse of the slope of the exponential function that best fits to the p_T distributions in the low-p_T region. PHENIX extracted the inverse slope parameter $T_{\rm eff}$ in two fit ranges for various centralities (see Figure 6, right plot). The inverse slope parameter is independent of the centrality but increases with increasing p_T. The possible explanation of this dependence is an increase in the early-time contribution with high temperature at larger p_T. This slope can be compared to the ALICE measurements in 0-20% centrality class Pb–Pb collisions at $\sqrt{s_{\rm NN}} = 2.76$ TeV in the fitting range $0.9 < p_T < 2.1$ GeV/c: $T_{\rm eff} = 297 \pm 12({\rm stat}) \pm 41({\rm syst})$ MeV. The temperature extracted at LHC is slightly greater than that obtained by PHENIX in Au–Au collisions at $\sqrt{s_{NN}} = 200$ GeV.

3.1. Direct Photon Elliptic Flow

Measurement of azimuthal anisotropy of particle production is a powerful tool to study initial conditions, time-space evolution and transport properties of the system. Collective flow is described with Fourier series coefficients v_n of particle yield with respect to the reaction plane angle. The elliptic flow, quantified by the second order coefficient, v_2 originates from the fact that the initial spacial anisotropy of the colliding nuclei is transformed to the final anisotropy in momentum space via strong interactions in the dense matter.

Direct photon elliptic flow was measured for the first time in Au–Au collisions at $\sqrt{s_{NN}}$ = 200 GeV by the PHENIX collaboration [32] and was found to be similar in magnitude to the elliptic flow of hadrons. This similarity can be explained neither with hydrodynamic nor with transport models, which commonly predict considerably lower values of v_2 for direct photons as a significant part of thermal photons, and is emitted at early times when the collective flow is still developing; see Figure 7. This finding, usually referred to as a "direct photon puzzle", is widely debated in the literature [33].

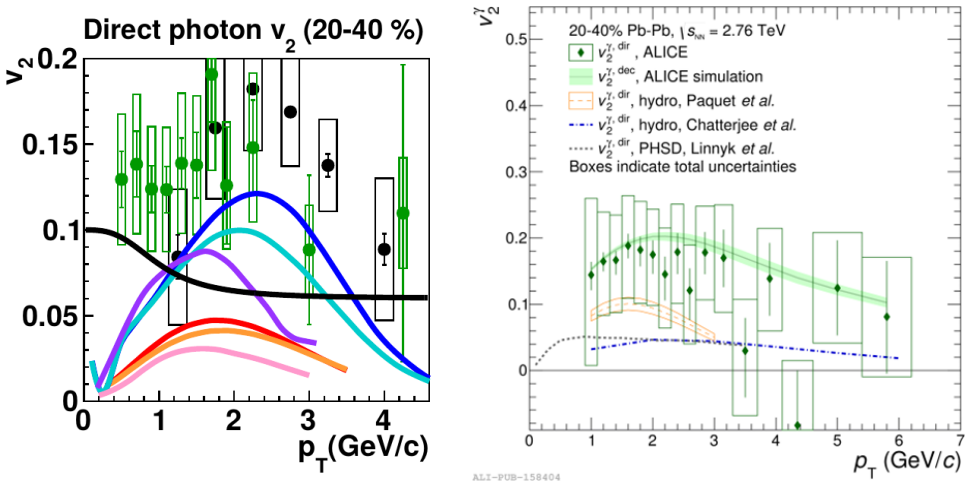

Figure 7. (**Left plot**): Direct photon flow v_2 measured in Au-Au collisions at $\sqrt{s_{NN}}$ = 200 GeV [34] with calorimeter (black) and photon conversion method (green), compared to phenomenological calculations (dark violet and cyan) [35], PHSD transport model (magenta) [36], magnetic field effect (black) [37], and hydrodynamic calculations (red, orange, and pink) [21,31]. (**Right plot**): the direct photon elliptic flow measured in Pb–Pb collisions at $\sqrt{s_{NN}}$ = 2.76 TeV [38] compared to the hydrodynamic [21,39] and PHSD transport model [40] calculations.

The ALICE collaboration measured the direct photon elliptic flow in Pb–Pb collisions at $\sqrt{s_{NN}}$ = 2.76 TeV in two centrality classes, 0–20% and 20–40% [38]; see Figure 7. The direct photon elliptic flow was found to be similar in magnitude to the elliptic flow of decay photons and systematically larger than predictions from hydrodynamic or transport models, although large systematic uncertainties of the measurements prevent us from drawing strong conclusions.

Several ideas were proposed to explain this puzzle. One of the most exciting models [41] predicts that the presence of a strong magnetic field at the very beginning of an A–A collision results in the creation of Landau levels for quarks and a characteristic dependence of the direct photon elliptic flow due to transitions between these levels: for sufficiently small $p_T \lesssim |eB|$, the elliptic flow of thermal photons becomes negative. This prediction differs from the one in any hydrodynamic or transport calculations that predict positive v_2 for any p_T. In order to discriminate between these scenarios, an extension of measurements to the lower p_T is required.

3.2. Direct Photons in Small Systems

One of the exciting open questions in the direct photon production is, do we observe thermal photon emission in small systems, such as pp or p–A collisions? How small can the system be to still be able to emit thermal photons? Prompt photon emission is clearly detected in all measured pp and p–A collisions, but it is not clear whether some excess of thermal photon emission at low p_T was observed. The PHENIX collaboration presented preliminary results on the direct photons' nuclear modification factor, defined as

$$R_{\mathrm{p+Au}} = \frac{dN^{\mathrm{p+Au}}_{\gamma,dir}/dp_T}{N_{\mathrm{coll}}\, dN^{\mathrm{pp}}_{\gamma,dir}/dp_T}$$

which shows some excess of direct photons at low p_T in the Minimum Bias and slightly more significant excess in 0–5% of the most central p–Au collisions [42]; see Figure 8. Both observed excesses are still within a 2σ deviation from the unity and should be considered as a hint of a possible physical effect.

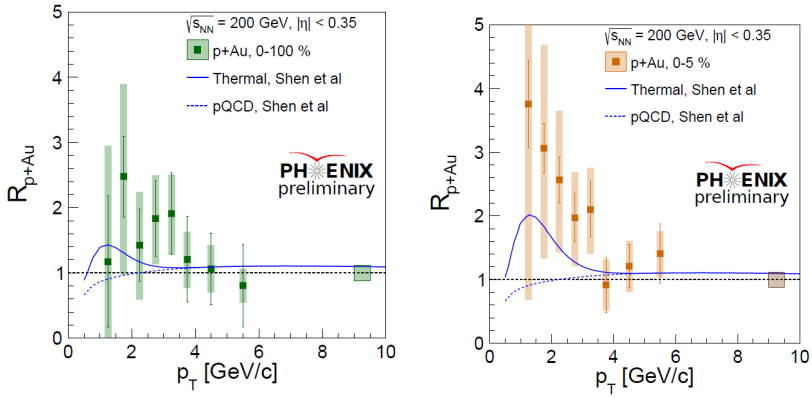

Figure 8. Nuclear modification factor $R_{\mathrm{p+Au}}$ for direct photon production in Minimum Bias (left) and 0–5% of the most central (right) p–Au collisions at $\sqrt{s_{\mathrm{NN}}} = 200$ GeV. Ref. [42] compared to predictions of hydrodynamic model [43].

The ALICE experiment measured direct photon excess $R_\gamma = N^{incl.}_\gamma / N^{decay}_\gamma$ as a function of the photon p_T in the Minimum Bias (left) and 0–20% of the most central (right) p–Pb collisions at $\sqrt{s_{\mathrm{NN}}} = 5.02$ TeV; see Figure 9. At high p_T, the observed excess over the unity agrees with the prompt photon contribution shown as NLO pQCD in the figure. However, at low p_T, the data agree both with the hydrodynamic calculation predicting the thermal photon yield (Shen et al. [44]) and with the unity, which corresponds to the absence of the thermal emission. So far, there is no clear evidence found of the thermal photon emission in small systems, such as the high-multiplicity pp or p–A collisions.

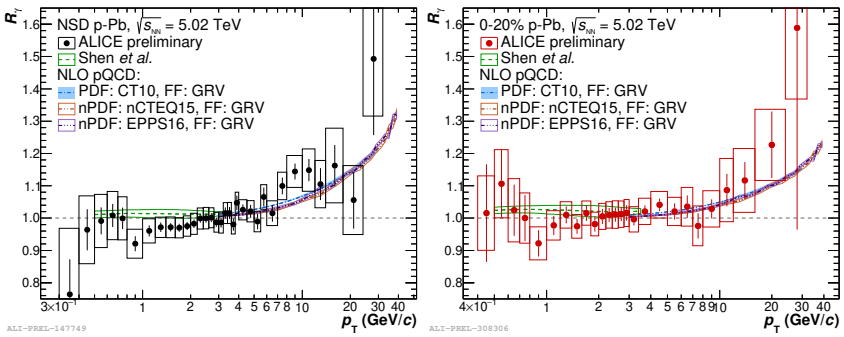

Figure 9. Direct photon excess $R_\gamma = N^{incl.}_\gamma / N^{decay}_\gamma$ as a function of photon p_T in Minimum Bias (**left**) and 0–20% of the most central (**right**) p–Pb collisions at $\sqrt{s_{\mathrm{NN}}} = 5.02$ TeV.

4. Direct Photons at Low Colliding Energies

Prompt photon production at NICA and FAIR energies will be a probe to structure functions in a high-x region, where they are relatively poorly constrained. To estimate uncertainties of the pQCD calculations of the prompt photon yield at NICA energies, we used Jetphox NLO pQCD calculations [9] with several recent parameterizations of the proton or nuclei structure functions; see Figure 10. The left plot represents the ratio of the prompt photon yield calculated using the proton structure functions (CT18 [45], NNPDF3.1 [46] and ABMP16 [47]) divided by the calculation with MMHT14 [48]. The right plot is the similar ratio but with ^{208}Pb nuclei structure functions nCTEQ15 [49], EPPS16 [50], nNNPDF2.0 [51] and TUJU16 [52]. At a low $p_T < 1$ GeV/c, the difference between predictions is modest and reaches a few tens of percents, but rapidly increases with p_T and can reach a factor of ~ 10 at $p_T \sim 1.5$ GeV/c. Therefore, measurements of prompt photons in pp collisions at NICA and FAIR energies will provide strong constraints for structure functions at high x.

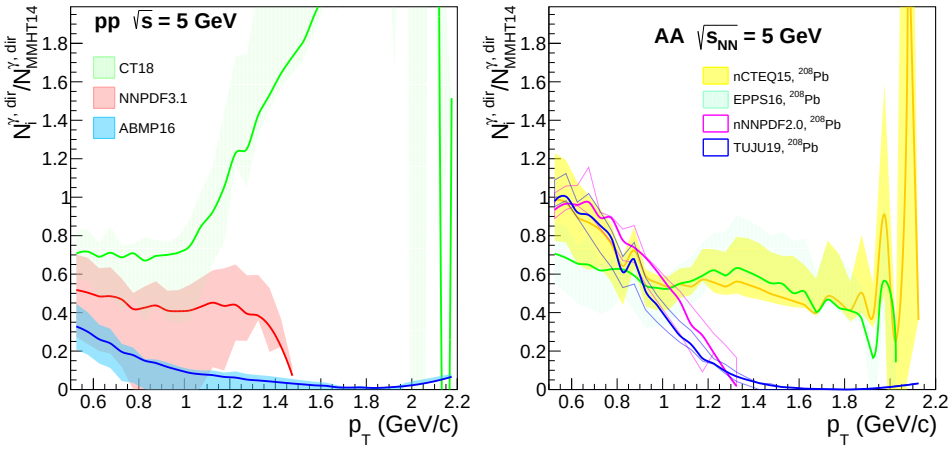

Figure 10. Ratio of prompt photon spectra calculated in pp (**left**) and A–A (**right**) collisions at $\sqrt{s_{NN}} = 5$ GeV with Jetphox package and several recent parameterizations of structure functions.

First, measurements of the direct photon production in relativistic heavy-ion collisions were performed in the experiment WA98 at SPS [53]. A large excess of the direct photon yield was observed, see Figure 11. Thanks to almost zero material budget between the calorimeter and the interaction point and fixed target setup of the experiment, this measurement covered a p_T range, from 0.5 to 4 GeV/c (providing only the upper limits of direct photon yield in the range $0.5 < p_T < 1.5$ GeV/c). Unfortunately, there is no measurement of direct photons in pp or p–A collisions at the same energy, and the WA98 collaboration had to scale the available data to the necessary energy. An excess of direct photons over the scaled p–A data was observed, which can be interpreted as the thermal photon emission.

To calculate the direct photon yield and collective flow of v_n for NICA and top FAIR energies ($\sqrt{s_{NN}}$= 5 and 11 GeV), we use a description of the dynamics of a heavy-ion collision with the Ultra-relativistic Quamtum Molecular Dynamics (UrQMD) model [54] version 3.4. This model uses the non-equilibrium dynamics of hadron strings in the initial state followed by a hadron re-scattering. An option to describe the thermalized system with ideal fluid dynamics is implemented within the latest versions of the UrQMD model [55]. In our calculations, the "Bag model" equation of state was used. It was shown in [56] that the contribution to the direct photon spectrum from the non-equilibrium initial stage and from the stage after the freeze-out in the p_T range below 3 GeV/c for the "Bag model" option is small. Direct photon production rates of the hadronic gas [57] and of the quark–gluon plasma [58] are implemented to evaluate the thermal photon yield. Finally, we verified that the model reproduces the thermal photon yield calculations for higher colliding energies [56,59] and in particular, reproduced WA98 measurements.

Spectra of direct photons, π^0 mesons, and decay photons calculated in Au–Au collisions at $\sqrt{s_{NN}} = 11$ and 5 GeV, are shown in Figure 12. The impact parameter for these simulations was distributed within the range $0 < b < 4.5$ fm, which corresponds to about 0–10% centrality. The blue band around the direct photon spectra represents the amount of event-by-event fluctuations (RMS) in the direct photon yield due to fluctuations of the initial state of the collision. The direct photon excess factor R_γ for the same collisions is presented in Figure 13. The expected excess of direct photons on the level of 3–5% is challenging, but, it is a realistic experimental task.

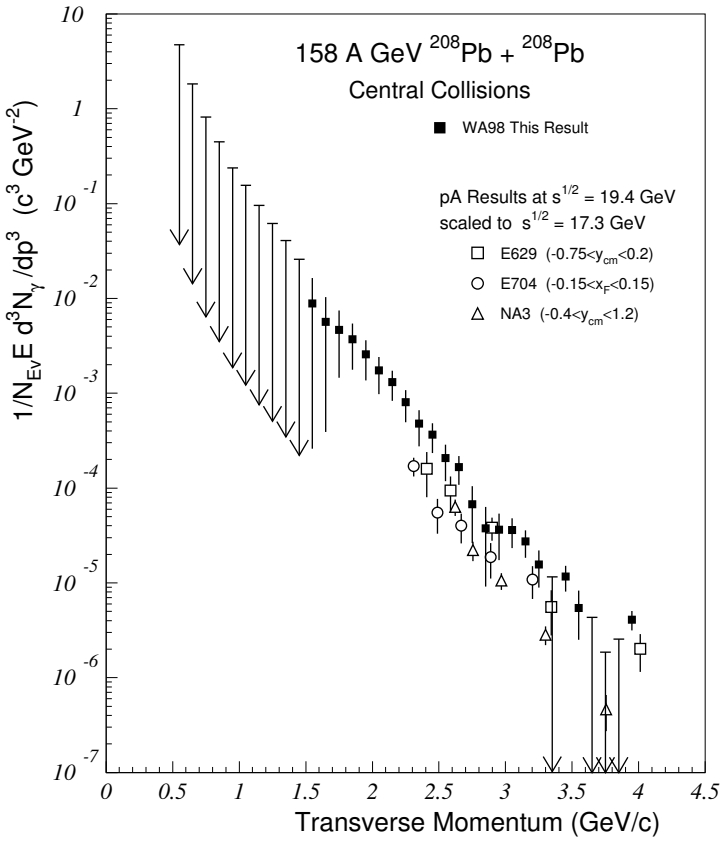

Figure 11. Direct photon spectrum measured in 20% central Pb–Pb collisions at $\sqrt{s_{NN}} = 17.3$ GeV.

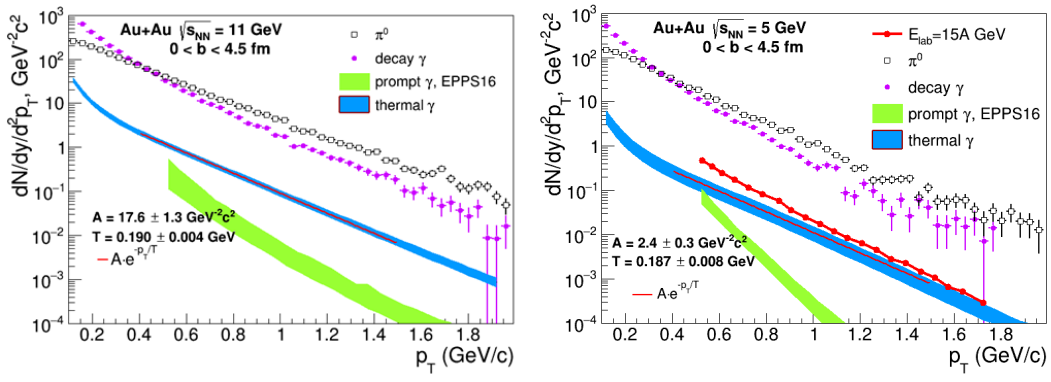

Figure 12. Simulated spectra of direct photons, spectra of π^0 mesons, and spectra of their decay photons in Au–Au collisions at $\sqrt{s_{NN}} = 11$ GeV (**left**) and 5 GeV (**right**). Impact parameter is generated within $0 < b < 4.5$ fm. Red points correspond to calculations of central Au–Au collisions at beam energy of $E_{lab} = 15A$ GeV from [59].

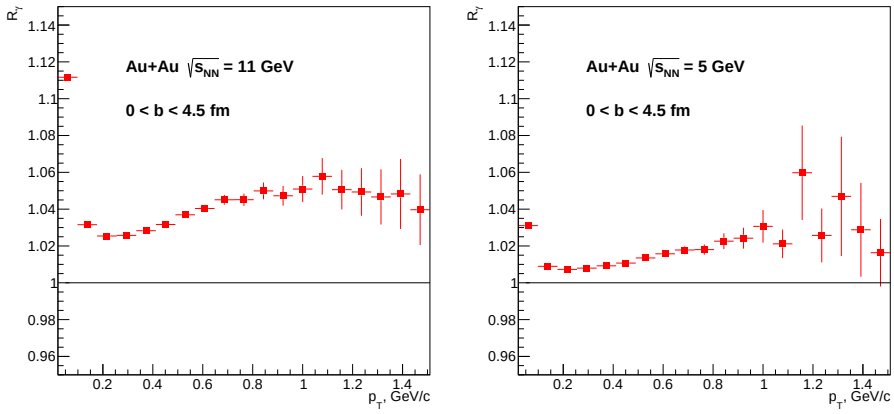

Figure 13. R_γ for Au–Au collisions at $\sqrt{s_{\rm NN}} = 11$ GeV (**left**) and $\sqrt{s_{\rm NN}} = 5$ GeV (**right**). Impact parameter is generated within $0 < b < 4.5$ fm.

The dependence of the directed and elliptic collective flow of direct photons v_1 and v_2 on rapidity is shown in Figures 14 and 15 for Au–Au collisions at $\sqrt{s_{\rm NN}} = 11$ and 5 GeV. The directed flow v_1 is found to have a similar dependence on the rapidity to the one predicted for charged hadrons (e.g., protons) at the same center-of-mass energies [60]. The blue bands represent the RMS of event-by-event variations of flow due to fluctuations in the initial state. Variations are found to be larger in collisions with $\sqrt{s_{\rm NN}} = 5$ GeV than for $\sqrt{s_{\rm NN}} = 11$ GeV. One of the interesting measurements at NICA would be to explore correlations between the direct photon and hadron directed and elliptic flow to trace how fluctuations in the initial state influence hadron collective flow.

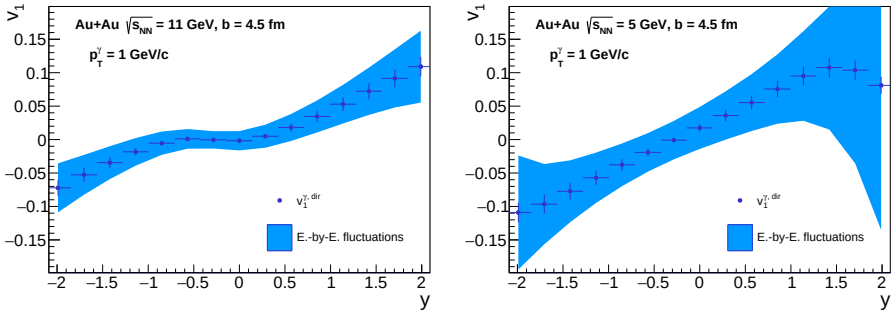

Figure 14. Directed flow $v_1(y)$ of direct photons at $p_{\rm T} = 1$ GeV/c for Au–Au collisions at $\sqrt{s_{\rm NN}} = 11$ (**left**) and 5 GeV (**right**). Blue bands shows RMS of the event-by-event fluctuations due to variation of the initial conditions.

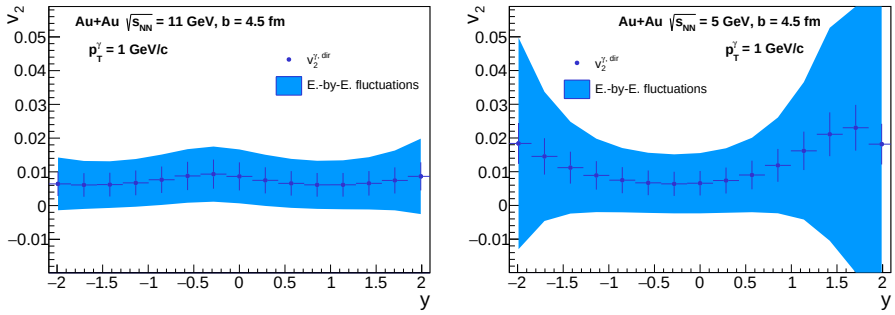

Figure 15. Elliptic flow $v_2(y)$ of direct photons at $p_{\rm T} = 1$ GeV/c for Au–Au collisions at $\sqrt{s_{\rm NN}} = 11$ (**left**) and 5 GeV (**right**). Blue bands shows RMS of the event-by-event fluctuations due to variation of the initial conditions.

5. Conclusions

Direct photons created in A–A collisions can be split into prompt and thermal photons. Prompt direct (as well as isolated) photon production is a powerful tool to test perturbative QCD predictions, parameterizations of structure functions, and control the initial state of A–A collisions. Measurements in pp and p–A collisions at low and high energies are consistent with NLO pQCD calculations. Thermal direct photons appear as an excess of direct photons over prompt direct photon contribution in the low-p_T range. Presently, WA98, PHENIX, and ALICE confirmed an excess of thermal radiation in A–A collisions and estimated the effective temperature of the quark–gluon plasma. No thermal photon excess in minimum bias or high multiplicity pp collisions was observed. Thermal photon excess in p–A collisions is not yet confirmed. The direct photon collective flow provides information on the evolution of the QGP and flow formation mechanisms: the direct photon elliptic flow measured by the PHENIX collaboration is large and not reproduced by hydrodynamic or transport models. A similar measurement of the ALICE collaboration seems to support this conclusion, but the uncertainties are too large to make a firm conclusion.

The results on direct photon production at NICA and FAIR energies are well anticipated. These measurements will provide constraints on proton and nuclear PDFs, signal about QGP formation through thermal photon excess and suggest possible hints for a critical point in the QCD phase diagram. We presented hybrid model calculations for direct photons' yield and flow at NICA and FAIR energies. Thermal direct photons excess at the top NICA energy ($\sqrt{s_{NN}}$= 11 GeV) is expected on the level of 5% in 0-10% centrality. Predictions for direct and elliptic flow of direct photons are also presented.

Author Contributions: Both authors equally contributed to all aspects of the paper. All authors have read and agreed to the published version of the manuscript.

Funding: This research was supported by NRC "Kurchatov Institute" and MEPhI program Priority 2030.

Institutional Review Board Statement: Not applicable.

Informed Consent Statement: Not applicable.

Data Availability Statement: Not applicable.

Acknowledgments: We acknowledge support from NRC "Kurchatov Institute" and NRNU "MEPhI".

Conflicts of Interest: The authors declare no conflict of interest.

References

1. Shuryak, E.V. Quark-Gluon Plasma and Hadronic Production of Leptons, Photons and Psions. *Phys. Lett. B* **1978**, *78*, 150. [CrossRef]
2. Afanasiev, S.; Aidala, C.; Ajitan, N.N.; Akiba, Y.; Al-Jamel, A.; Alex, J.; Aoki, K.; Aphecetche, L.; Armendariz, R.; Aronson, S.H.; et al. Measurement of Direct Photons in Au+Au Collisions at $\sqrt{s_{NN}} = 200$ GeV. *Phys. Rev. Lett.* **2012**, *109*, 152302. [CrossRef] [PubMed]
3. Bock, F. Shining a Light on the QGP—Electroweak Probes Experimental Summary. *PoS* **2019**, *HardProbes2018*, 011. [CrossRef]
4. Wilson, K.G. Nonlagrangian models of current algebra. *Phys. Rev.* **1969**, *179*, 1499–1512. [CrossRef]
5. Berman, S.M.; Bjorken, J.D.; Kogut, J.B. Inclusive Processes at High Transverse Momentum. *Phys. Rev. D* **1971**, *4*, 3388–3418. [CrossRef]
6. Arleo, F.m.c.; Brodsky, S.J.; Hwang, D.S.; Sickles, A.M. Higher-Twist Dynamics in Large Transverse Momentum Hadron Production. *Phys. Rev. Lett.* **2010**, *105*, 062002. [CrossRef]
7. Contogouris, A.P.; Kamal, B.; Merebashvili, Z.; Tkachov, F.V. Complete next-to-leading order corrections for direct photon production by polarized beam and target. *Phys. Lett. B* **1993**, *304*, 329–333. [CrossRef]
8. Gordon, L.; Vogelsang, W. Polarized and unpolarized prompt photon production beyond the leading order. *Phys. Rev.* **1993**, *D48*, 3136–3159. [CrossRef] [PubMed]
9. Catani, S.; Fontannaz, M.; Guillet, J.P.; Pilon, E. Cross-section of isolated prompt photons in hadron hadron collisions. *JHEP* **2002**, *2002*, 028. [CrossRef]

10. Aurenche, P.; Fontannaz, M.; Guillet, J.P.; Pilon, E.; Werlen, M. A New critical study of photon production in hadronic collisions. *Phys. Rev. D* **2006**, *73*, 094007. [CrossRef]
11. Aurenche, P.; Basu, R.; Fontannaz, M. NLO Calculation of Prompt Photon Production in DIS at HERA. *Eur. Phys. J. C* **2011**, *71*, 1616. [CrossRef]
12. Bothmann, E.; Singh, C.G.; Höche, S.; Krause, J.; Krauss, F.; Kuttimalai, S.; Liebschner, S.; Napoletano, D.; Schönherr, M.; Schulz, H.; et al. Event Generation with Sherpa 2.2. *SciPost Phys.* **2019**, *7*, 034. [CrossRef]
13. Chen, X.; Gehrmann, T.; Glover, N.; Höfer, M.; Huss, A. Isolated photon and photon+jet production at NNLO QCD accuracy. *JHEP* **2020**, *4*, 166. [CrossRef]
14. Miller, M.L.; Reygers, K.; Sanders, S.J.; Steinberg, P. Glauber modeling in high energy nuclear collisions. *Ann. Rev. Nucl. Part. Sci.* **2007**, *57*, 205–243. [CrossRef]
15. Abbott, B.; Abdallah, J.; Khalek, S.A.; Abdinov, O.; Aben, R.; Abi, B.; Abolins, M.; AbouZeid, O.; Abramowicz, H.; Abreu, H.; et al. Centrality, rapidity and transverse momentum dependence of isolated prompt photon production in lead-lead collisions at $\sqrt{s_{\mathrm{NN}}} = 2.76$ TeV measured with the ATLAS detector. *Phys. Rev. C* **2016**, *93*, 034914. [CrossRef]
16. Chatrchyan, S.; Khachatryan, V.; Sirunyan, A.M.; Tumasyan, A.; Adam, W.; Bergauer, T.; Dragicevic, M.; Erö, J.; Fabjan, C.; Friedl, M.; et al. Measurement of isolated photon production in pp and PbPb collisions at $\sqrt{s_{NN}} = 2.76$ TeV. *Phys. Lett. B* **2012**, *710*, 256–277. [CrossRef]
17. Aad, G.; Abbott, D.C.; Abdinov, O.; Abeling, K.; Abidi, S.H.; Abraham, N.L.; Abreu, H.; Adamek, L.; Adam, L.; Adelman, J.; et al. Measurement of the inclusive isolated-photon cross section in pp collisions at $\sqrt{s} = 13$ TeV using 36 fb^{-1} of ATLAS data. *JHEP* **2019**, *10*, 203. [CrossRef]
18. Acharya, S.; Adamová, D.; Adhya, S.P.; Adler, A.; Adolfsson, J.; Aggarwal, M.M.; Aglieri Rinella, G.; Agnello, M.; Agrawal, N.; Ahammed, Z.; et al. Measurement of the inclusive isolated photon production cross section in pp collisions at $\sqrt{s} = 7$ TeV. *Eur. Phys. J. C* **2019**, *79*, 896. [CrossRef]
19. Adare, A.; Afanasiev, S.; Aidala, C.; Ajitan, N.N.; Akiba, Y.; Al-Bataineh, H.; Alex, J.; Al-Jamel, A.; Aoki, K.; Aphecetche, L.; et al. Enhanced production of direct photons in Au+Au collisions at $\sqrt{s_{NN}} = 200$ GeV and implications for the initial temperature. *Phys. Rev. Lett.* **2010**, *104*, 132301. [CrossRef]
20. Adam, J.; Adamová, D.; Aggarwal, M.M.; Rinella, G.A.; Agnello, M.; Agrawal, N.; Ahammed, Z.; Ahn, S.U.; Aiola, S.; Akindinov, A.; et al. Direct photon production in Pb-Pb collisions at $\sqrt{s_{NN}} = 2.76$ TeV. *Phys. Lett. B* **2016**, *754*, 235–248. [CrossRef]
21. Paquet, J.F.; Shen, C.; Denicol, G.S.; Luzum, M.; Schenke, B.; Jeon, S.; Gale, C. Production of photons in relativistic heavy-ion collisions. *Phys. Rev. C* **2016**, *93*, 044906. [CrossRef]
22. van Hees, H.; He, M.; Rapp, R. Pseudo-critical enhancement of thermal photons in relativistic heavy-ion collisions? *Nucl. Phys. A* **2015**, *933*, 256–271. [CrossRef]
23. Chatterjee, R.; Holopainen, H.; Renk, T.; Eskola, K.J. Collision centrality and τ_0 dependence of the emission of thermal photons from fluctuating initial state in ideal hydrodynamic calculation. *Phys. Rev. C* **2012**, *85*, 064910. [CrossRef]
24. Bratkovskaya, E.L.; Cassing, W.; Moreau, P.; Soloveva, O.E.; Oliva, L.; Song, T. PHSD—A microscopic transport approach for strongly interacting systems. In *Advances in Nuclear Physics*; Structure and Reactions; Springer: Singapore, 2021; pp. 119–136.
25. Acharya, U.A.; Adare, A.; Aidala, C.; Ajitan, N.N.; Akiba, Y.; Alfred, M.; Apadula, N.; Asano, H.; Azmoun, B.; Babintsev, V.; et al. Nonprompt direct-photon production in Au+Au collisions at $\sqrt{s_{NN}} = 200$ GeV. *arXiv* **2022**, arXiv:2203.17187.
26. Adamczyk, L.; Adkins, J.K.; Agakishiev, G.; Aggarwal, M.M.; Ahammed, Z.; Ajitan, N.N.; Alekseev, I.; Anderson, D.M.; Aoyama, R.; Aparin, A.; et al. Direct virtual photon production in Au+Au collisions at $\sqrt{s_{NN}}$ = 200 GeV. *Phys. Lett. B* **2017**, *770*, 451–458. [CrossRef]
27. Adare, A.; Afanasiev, S.; Aidala, C.; Ajitan, N.N.; Akiba, Y.; Al-Bataineh, H.; Alex, J.; Al-Jamel, A.; Aoki, K.; Aphecetche, L.; et al. Detailed measurement of the e^+e^- pair continuum in $p+p$ and Au+Au collisions at $\sqrt{s_{NN}} = 200$ GeV and implications for direct photon production. *Phys. Rev. C* **2010**, *81*, 034911. [CrossRef]
28. Kroll, N.M.; Wada, W. Internal pair production associated with the emission of high-energy gamma rays. *Phys. Rev.* **1955**, *98*, 1355–1359. [CrossRef]
29. Gale, C.; Paquet, J.F.M.C.; Schenke, B.; Shen, C. Multimessenger heavy-ion collision physics. *Phys. Rev. C* **2022**, *105*, 014909. [CrossRef]
30. Adare, A.; Afanasiev, S.; Aidala, C.; Ajitan, N.N.; Akiba, Y.; Akimoto, R.; Al-Bataineh, H.; Alex, J.; Alfred, M.; Al-Jamel, A.; et al. Beam Energy and Centrality Dependence of Direct-Photon Emission from Ultrarelativistic Heavy-Ion Collisions. *Phys. Rev. Lett.* **2019**, *123*, 022301. [CrossRef]
31. Shen, C.; Heinz, U.W.; Paquet, J.F.; Gale, C. Thermal photons as a quark-gluon plasma thermometer reexamined. *Phys. Rev. C* **2014**, *89*, 044910. [CrossRef]
32. Adare, A.; Afanasiev, S.; Aidala, C.; Ajitan, N.N.; Akiba, Y.; Al-Bataineh, H.; Alex, J.; Aoki, K.; Aramaki, Y.; Atomssa, E.T.; et al. Observation of direct-photon collective flow in $\sqrt{s_{NN}} = 200$ GeV Au+Au collisions. *Phys. Rev. Lett.* **2012**, *109*, 122302. [CrossRef] [PubMed]

33. David, G. Direct real photons in relativistic heavy ion collisions. *Rept. Prog. Phys.* **2020**, *83*, 046301. [CrossRef] [PubMed]
34. Mizuno, S. Centrality dependence of soft photon production and its collective flow in Au+Au collisions at $\sqrt{s_{NN}} = 200$ GeV. *Nucl. Phys. A* **2014**, *931*, 686–690. [CrossRef]
35. van Hees, H.; Gale, C.; Rapp, R. Thermal Photons and Collective Flow at the Relativistic Heavy-Ion Collider. *Phys. Rev. C* **2011**, *84*, 054906. [CrossRef]
36. Linnyk, O.; Cassing, W.; Bratkovskaya, E.L. Centrality dependence of the direct photon yield and elliptic flow in heavy-ion collisions at $\sqrt{s_{NN}} = 200$ GeV. *Phys. Rev. C* **2014**, *89*, 034908. [CrossRef]
37. Muller, B.; Wu, S.Y.; Yang, D.L. Elliptic flow from thermal photons with magnetic field in holography. *Phys. Rev. D* **2014**, *89*, 026013. [CrossRef]
38. Acharya, S.; Adamová, D.; Adolfsson, J.; Aggarwal, M.M.; Rinella, G.A.; Agnello, M.; Agrawal, N.; Ahammed, Z.; Ahn, S.U.; Aiola, S.; et al. Direct photon elliptic flow in Pb-Pb collisions at $\sqrt{s_{\rm NN}}$ = 2.76 TeV. *Phys. Lett. B* **2019**, *789*, 308–322. [CrossRef]
39. Chatterjee, R.; Srivastava, D.K. Elliptic flow of thermal photons and formation time of quark gluon plasma at RHIC. *Phys. Rev. C* **2009**, *79*, 021901. [CrossRef]
40. Linnyk, O.; Bratkovskaya, E.L.; Cassing, W. Effective QCD and transport description of dilepton and photon production in heavy-ion collisions and elementary processes. *Prog. Part. Nucl. Phys.* **2016**, *87*, 50–115. [CrossRef]
41. Wang, X.; Shovkovy, I.A.; Yu, L.; Huang, M. Ellipticity of photon emission from strongly magnetized hot QCD plasma. *Phys. Rev. D* **2020**, *102*, 076010. [CrossRef]
42. Novitzky, N. Low-p_T direct photon production in $p + p$ and $p+$ Au collisions at $\sqrt{s_{\rm NN}}$ = 200 GeV. *PoS* **2019**, *HardProbes2018*, 185. [CrossRef]
43. Shen, C.; Paquet, J.F.; Denicol, G.S.; Jeon, S.; Gale, C. Electromagnetic radiation and collectivity in small quark–gluon droplets. *Nucl. Part. Phys. Proc.* **2017**, *289–290*, 161–164. [CrossRef]
44. Shen, C.; Paquet, J.F.; Denicol, G.S.; Jeon, S.; Gale, C. Collectivity and electromagnetic radiation in small systems. *Phys. Rev. C* **2017**, *95*, 014906. [CrossRef]
45. Hou, T.J.; Gao, J.; Hobbs, T.J.; Xie, K.; Dulat, S.; Guzzi, M.; Huston, J.; Nadolsky, P.; Pumplin, J.; Schmidt, C.; et al. New CTEQ global analysis of quantum chromodynamics with high-precision data from the LHC. *Phys. Rev. D* **2021**, *103*, 014013. [CrossRef]
46. Ball, R.D.; Bertone, V.; Carrazza, S.; Debbio, L.D.; Forte, S.; Groth-Merrild, P.; Guffanti, A.; Hartl, N.P.; Kassabov, Z.; Latorre, J.I.; et al. Parton distributions from high-precision collider data. *Eur. Phys. J. C* **2017**, *77*, 663. [CrossRef]
47. Alekhin, S.; Blümlein, J.; Moch, S.; Placakyte, R. Parton distribution functions, α_s, and heavy-quark masses for LHC Run II. *Phys. Rev. D* **2017**, *96*, 014011. [CrossRef]
48. Harland-Lang, L.A.; Martin, A.D.; Motylinski, P.; Thorne, R.S. Parton distributions in the LHC era: MMHT 2014 PDFs. *Eur. Phys. J. C* **2015**, *75*, 204. [CrossRef]
49. Kusina, A.; Kovarik, K.; Jezo, T.; Clark, D.B.; Keppel, C.; Lyonnet, F.; Morfin, J.G.; Olness, F.I.; Owens, J.F.; Schienbein, I.; et al. nCTEQ15—Global analysis of nuclear parton distributions with uncertainties in the CTEQ framework. *Phys. Rev. D* **2016**, *93*, 085037. [CrossRef]
50. Eskola, K.J.; Paakkinen, P.; Paukkunen, H.; Salgado, C.A. EPPS16: Nuclear parton distributions with LHC data. *Eur. Phys. J. C* **2017**, *77*, 163. [CrossRef]
51. Abdul Khalek, R.; Ethier, J.J.; Rojo, J. Nuclear parton distributions from lepton-nucleus scattering and the impact of an electron-ion collider. *Eur. Phys. J. C* **2019**, *79*, 471. [CrossRef]
52. Alekhin, S.; Blümlein, J.; Moch, S. NLO PDFs from the ABMP16 fit. *Eur. Phys. J. C* **2018**, *78*, 477. [CrossRef]
53. Aggarwal, M.M.; Agnihotri, A.; Ahammed, Z.; Angelis, A.L.S.; Antonenko, V.; Arefiev, V.; Astakhov, V.; Avdeitchikov, V.; Awes, T.C.; et al. Observation of direct photons in central 158-A-GeV Pb-208 + Pb-208 collisions. *Phys. Rev. Lett.* **2000**, *85*, 3595–3599. [CrossRef] [PubMed]
54. Bass, S.A.; Belkacem, M.; Bleicher, M.; Bravina, L.; Ernst, C.; Gerl, L.; Hofmann, M.; Hofmann, S.; Konopka, J.; Mao, G.; et al. Microscopic models for ultrarelativistic heavy ion collisions. *Prog. Part. Nucl. Phys.* **1998**, *41*, 255–369. [CrossRef]
55. Petersen, H.; Steinheimer, J.; Burau, G.; Bleicher, M.; Stöcker, H. A Fully Integrated Transport Approach to Heavy Ion Reactions with an Intermediate Hydrodynamic Stage. *Phys. Rev. C* **2008**, *78*, 044901. [CrossRef]
56. Bäuchle, B.; Bleicher, M. Hybrid model calculations of direct photons in high-energy nuclear collisions. *Phys. Rev. C* **2010**, *81*, 044904. [CrossRef]
57. Turbide, S.; Rapp, R.; Gale, C. Hadronic production of thermal photons. *Phys. Rev. C* **2004**, *69*, 014903. [CrossRef]
58. Arnold, P.B.; Moore, G.D.; Yaffe, L.G. Photon emission from quark gluon plasma: Complete leading order results. *JHEP* **2001**, *12*, 009. [CrossRef]

59. Endres, S.; van Hees, H.; Bleicher, M. Photon and dilepton production at the Facility for Antiproton and Ion Research and beam-energy scan at the Relativistic Heavy-Ion Collider using coarse-grained microscopic transport simulations. *Phys. Rev. C* **2016**, *93*, 054901. [CrossRef]
60. Parfenov, P.; Taranenko, A.; Selyuzhenkov, I.; Senger, P. Performance studies of anisotropic flow with MPD at NICA. *EPJ Web Conf.* **2019**, *204*, 07010. [CrossRef]